minerals

MDPI

Article

Comparison of Geometric Properties of Regular and Irregular Mineral Grains by Dynamic Image Analysis (2D) and Optoelectronic Analysis (3D) Methods

Damian Krawczykowski, Aldona Krawczykowska * and Tomasz Gawenda

Department of Environmental Engineering, Faculty of Civil Engineering and Resource Management, AGH University of Science and Technology, 30-059 Cracow, Poland; dkrawcz@agh.edu.pl (D.K.); gawenda@agh.edu.pl (T.G.)

* Correspondence: aldona.krawczykowska@agh.edu.pl

Abstract: The properties of bulk materials are influenced by geometrical features of grains such as size, size distribution and shape. However, size is an ambiguous parameter for non-spherical particles. Therefore, the influence of the shape of a particle on its size, as described by various measuring methods and estimators using the main particle dimensions, was studied here. Granulometric analyses of mineral raw material samples containing regular and irregular grains were performed as part of the research. The measurements were made using two methods: the dynamic image analysis and the optoelectronic analysis. The main dimensions of the particles in 2D and 3D space were measured. Particle shape descriptors were determined based on the measurements: circularity and sphericity. Particle size distributions were also determined as a function of the minimum and maximum Feret diameters (for the 2D method) and the shortest and longest dimensions of particles recorded by the 3D method. The distribution of grain shapes according to Zingg classification was used for the 3D method. The results of the study were discussed in the context of comparing both of the measuring methods and selecting the most appropriate one to assess particle (ir)regularity.

Keywords: particle shape analysis; 2D and 3D measurement methods; dynamic image analysis; optoelectronic method

check for updates

Citation: Krawczykowski, D.; Krawczykowska, A.; Gawenda, T. Comparison of Geometric Properties of Regular and Irregular Mineral Grains by Dynamic Image Analysis (2D) and Optoelectronic Analysis (3D) Methods. *Minerals* **2022**, *12*, 540. https://doi.org/10.3390/min12050540

Academic Editors: Chiharu Tokoro, Shigeshi Fuchida and Yutaro Takaya

Received: 7 March 2022
Accepted: 25 April 2022
Published: 27 April 2022

Publisher's Note: MDPI stays neutral with regard to jurisdictional claims in published maps and institutional affiliations.

Copyright: © 2022 by the authors. Licensee MDPI, Basel, Switzerland. This article is an open access article distributed under the terms and conditions of the Creative Commons Attribution (CC BY) license (https://creativecommons.org/licenses/by/4.0/).

1. Introduction

The shape and size of particles plays an important role in the behavior of granular materials in various engineering applications. Therefore, the characterization and proper quantification of particle geometry are essential for understanding the properties of granular materials.

The assessment of the sizes and shapes of irregular particles, especially flatness, is a key issue in many fields of science. According to two standards, EN 933-3:2012 [1] and EN933-4:2008 [2], flat grains are classified as those for which the ratio of the largest dimension (length) to the smallest dimension (thickness) is equal to or larger than 3. Flatness affects the strength of particles as such and that of the structures formed by them [3–14]. The flat shape of particles causes disturbances in their flow in liquids or gases, which affects the speed and stability of the movement of grains in liquid medium [15,16]. This translates into indicators of sharpness of grain separation in such media, e.g., in hydraulic and pneumatic separators or jigs, and also affects the rate of grain sedimentation in thickening processes [17–19]. There are also many studies in which their authors show the influence of the shape of grains on the results of measurements of their size using various measurement techniques [20–23].

The particle size and shape are the basic physical parameters that characterize bulk materials. At the same time, the shape of a grain is a conventional concept, since it can be determined in different ways according to different classifications or using different shape

factors and measurement techniques [24–30]. Although there is an extensive literature on the subject, no common optimal method of classifying shapes of mineral grains has been selected [31,32].

Contemporary tools used to determine the geometric properties of particles include vision systems with computer image analysis, often supported by artificial intelligence techniques [33–35]. They use, among others, such measurement techniques as optical microscopy, dynamic image analysis (DIA), the optoelectronic method, scanning electron microscopy (SEM), X-ray micro-computed tomography (micro-CT) and laser scanning (LS), which offer various possibilities for measuring the sizes and shapes of particles. Each of these techniques generates information about the object that is characteristic of the specific measuring method. They enable 2D or 3D imaging, which significantly differentiates information on particle geometry, morphology and surface texture [36–51].

2. Materials and Methods

2.1. Purpose and Scope of the Research

Measurements of particle sizes and shapes were made on mineral samples of chalcedonite using two different measuring methods: dynamic image analysis (2D) and optoelectronic analysis (3D). The samples contained regular (Reg) and irregular (Irr) grains classified using slotted sieves in a narrow grain class of 6.3–8 mm. There were two feeds (Feed Reg and Feed Irr) and two pairs of four products of their enrichment in a hydraulic jig (I–IV Reg and I–IV Irr). The method of their enrichment and the impact of this process on the physico-chemical properties of the grains was not the subject of this study. This method has been discussed in earlier publications by the authors [52,53]. The population of measured and analyzed grains in the tested samples was comparable: about 1500.

In this research work, we proposed a new approach for comparing grain size distributions and grain shapes determined by different measuring methods. The approach consisted of comparing grain size distribution estimators and grain shape descriptors suitable for a given measuring method: 2D class estimator for the dynamic image analysis and 3D class estimator for the optoelectronic method. Thus, the aim of the study was to compare the effectiveness of identifying grains that are substantially different in their geometries (regular and irregular) with these two measuring methods using appropriate evaluation indicators. Two well-known shape descriptors based on the main dimensions of grains were used for this purpose: circularity (2D descriptor) and sphericity (3D descriptor). The circularity descriptor was used to describe the shapes of the grains measured by the dynamic 2D image analysis, while the sphericity descriptor was used to describe the shapes of the grains measured by the 3D optoelectronic method. Functional dependencies between the estimators and coefficients of determination R2 were established to study the correspondence of these descriptors. The distribution of grain shapes defined according to Zingg classification was determined for the 3D measuring method. In addition to comparing the distributions of grain shapes, the distributions of their sizes were also compared based on their shortest and their longest dimensions. The minimum and maximum diameters (d_{Fmin}, d_{Fmax}) were used for the 2D measuring method and the particle width (b) and length (a) for the 3D method. Span was the estimator of the grain size distribution, which is a measure of the width and skewness of the distribution [47]. The results of the measurements were presented in the form of cumulative particle size distributions and particle shape expressed by volume (Q3-particles volume density distribution).

2.2. Shape Descriptors

To characterize the shape of a particle, shape descriptors are used—mathematical functions using previously measured dimensions (dimensional variables) of particles such as length, diameter, circumference, surface area or volume. These functions can be divided into 1D, 2D and 3D shape descriptors depending on the variables and measuring methods used [54]. The 1D class of shape descriptors are simple and well-known shape factors, such as the flatness, elongation or the proportionality factor, which can be easily measured. The

2D shape descriptors are based on 2D variables determined by analyzing the images of particle projections. Examples of 2D variables include projection circumferences, surface areas and diameters of incircles and circumcircles of particles, or the circularity shape factor. The 3D shape descriptors describe the 3D space of a particle. An example of such a descriptor is sphericity based on the principal dimensions of particles, such as the volume, surface area, minimum circumscribed sphere, maximum inscribed sphere and the 3D convex hull [45,55–60].

Two shape descriptors were used in this study: the 2D circularity and the 3D sphericity. Conventionally, the sphericity is defined as the ratio between the surface area of a sphere of the same volume as the particle and the surface area of the particle [61]. It therefore quantifies to what extent the shape of the particle is similar to the shape of the sphere. It is therefore a subjective method of measuring the sphericity of particles. While the volume of particles can be calculated using Archimedes' weight method, determining the surface of the particles—especially irregular ones with rough surfaces—can be problematic [62]; in this case, the surface area is also usually underestimated. This is why Krumbein has proposed his own measure of sphericity—this measure is based only on the triaxial dimensions of the particle [25]:

$$S = \sqrt[3]{\frac{c \cdot b}{a^2}} \quad (1)$$

where c, b and a—c the intermediate, shortest, and longest dimension of the ellipsoid axial dimensions, respectively.

Other authors agreed with this measure while Bullard and Garboczi argued that the sphericity should be based either on the relation of the limiting spheres or on their triaxial dimensions [45].

Figure 1 shows the spatial dimensioning of the grain according to the determinations of its main dimensions, used to calculate the sphericity factor S.

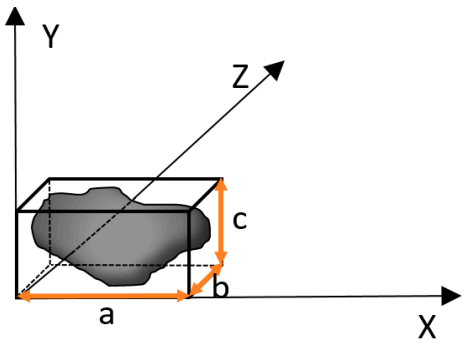

Figure 1. The determination of the basic grain dimensions.

The definition of the circularity of a particle, originally proposed by Cox [63], compares the particle's surface area to its circumference. If the surface area and circumference do not change, the circularity is constant. Thus, as the value of the circularity factor decreases, the particle becomes more irregular. The circularity factor C was defined in this study as the ratio of the total surface area of the particle to the Crofton parameter, according to the formula:

$$C = \frac{4\pi D}{P_c^2} \quad (2)$$

where D—the particle's surface area; P_C—the normalized measure of the number of edges of 0°, 45°, 90° and 135° in the object (Crofton parameter).

2.3. Measurement Methods

2.3.1. 2D Imaging

The 2D measurements of particle size and shape were carried out using a vision system employing the dynamic image analysis (DIA) technique. The principle for operating the vision system consisted of filming moving particles followed by computer-aided analysis of their images (the shape and size of each particle separately) using dedicated software. The Analysette 28 ImageSizer granulometer (Fritsch GMBH, Germany) was used for the study. This device generates a stroboscopic effect using a pulsing light source, a high-speed video camera and interchangeable optical systems. The vision system captures images of particles in motion at speeds of up to several hundred objects per second. The measurement was performed on dry particles falling gravitationally in front of the camera lens (Figure 2). This was performed as a free fall, so the orientation of the particles was random. Their actual shapes and grain size distribution could be determined from different perspectives. Thanks to this method of measurement, about ten thousand images per minute were analyzed. The large number of filmed particles produced reliable and representative measurement results with a high level of confidence. This measurement technique is based on ISO 13322-2.

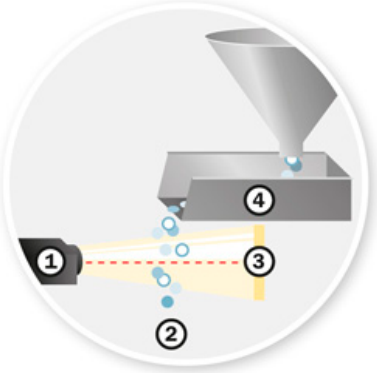

Figure 2. The dynamic image analysis (DIA) method of measuring particle sizes and shapes. 1—camera, 2—measurement volume, 3—light source, 4—feeder (source: www.fritsch-international.com/particle-sizing/fritsch-knowledge/dynamic-image-analysis/ (accessed on 22 January 2022)).

2.3.2. 3D Imaging

Accurate data on the volume and surface area of particles are currently provided by 3D techniques—e.g., laser scanning (LS), computed tomography (CT)—which make it possible to reliably reconstruct the external geometries of particles. However, these are complicated and inefficient methods for the online estimation of particle size distributions and shapes. They are based, among others, on numerical algorithms using the concept of principal component analysis (PCA) and the empirical cumulative distribution function (ECDF), or convexity and concavity descriptors [64,65]. It is also a problem to extract effective quantitative parameters of a shape from such detailed 3D images of particles. In general, three main methods for the qualitative description of such detailed characteristics of 3D particles can be distinguished: direct calculations for a set of image voxels, calculations using the spherical harmonic function, and calculations based on the local curvature on a reconstructed triangular surface mesh [66].

The complexity of these methods encourages the search for simplified, fast and easy-to-use 3D methods, though they often generate approximate information on the 3D shapes of grains. The optoelectronic method used in this study is such a 3D measurement technique. It uses one of the oldest methods of describing grain shapes: Zingg classification, which divides grains into spheres, disks, rods and blades [27]. Zingg has proposed the approximation of grains using the triaxial ellipsoid, and the classification of shapes based on the relations between the three dimensions of mutually perpendicular grains on the coordinate axis.

The 3D measurements of particle size and shape were carried out using an optoelectronic AWK 3D analyzer (Figure 3). These measurements were based on the principle of scatter of infrared light flux by a particle moving within the measuring space. The measuring space consists of two separate measuring probes, each containing a photodiode and a detector which are perpendicular to each other. This is how the particle passing through the measuring space is measured in two perpendicular directions, while the third dimension is determined on the basis of the time-of-passage of the particle through the measuring space. The particle passing in front of the detector absorbs light and the change in the intensity of the light flux reaching the detector is reflected in the amplitude of the electrical signal. The electrical impulse is then converted from electric units to metric units by an A/D converter, which corresponds to the size of the passing particle, and the precisely measured number of impulses is converted into the number of particles measured. The optical transducer consists of a photodiode (1) illuminating the optical system (2) which forms a parallel light beam (3) with a thickness of several hundred micrometers (Figure 4). The measuring space is contained between the optical systems (2) and (4). The optical system (4) focuses the radiation of the scattered beam (3) on the photoelement (5). If a grain passes through the measuring space, it will cause radiation to dissipate and change the intensity of the current flowing through the photosensitive element. The change in intensity will be proportional to the size of the falling grain.

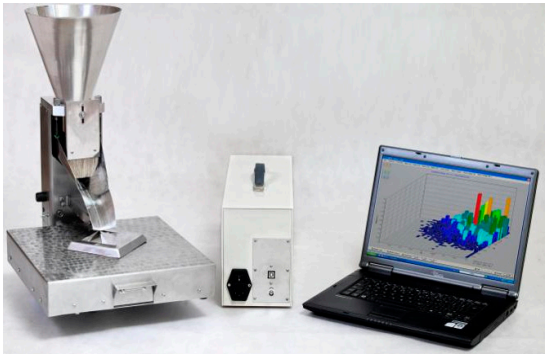

Figure 3. The AWK 3D Analyzer (source: www.kamika.pl/en/AWK_3D (accessed on 20 January 2022)).

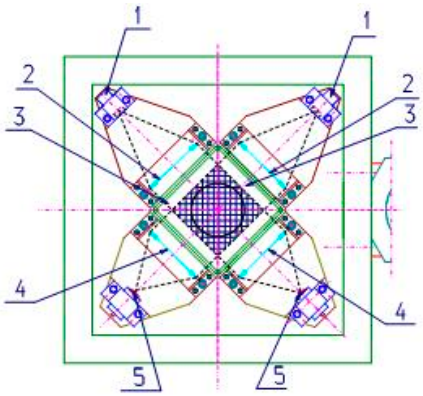

Figure 4. The optical transducer of the AWK 3D Analyzer (source: www.kamika.pl/Analizator_P_AWK3D (accessed on 20 January 2022)).

The analyzer therefore makes it possible to measure the sizes and shapes of grains. Each particle is measured simultaneously in three dimensions, where a is the length of the particle, b is width and c is thickness. The software then analyzes the relationships between the three dimensions of each particle and classifies its shape according to Zingg's characteristics as spheres, disks, rods or blades. Based on this classification, the flatness coefficient—as the ratio of dimensions (c/b)—and the elongation coefficient (b/a) are

determined. These coefficients group particle shapes according to the following proportions: disks ($b/a > 2/3$ and $c/b < 2/3$), spheres ($b/a > 2/3$ and $c/b > 2/3$), blades ($b/a < 2/3$ and $c/b < 2/3$) and rods ($b/a < 2/3$ and $c/b > 2/3$). The volumetric distribution of the particle shapes is presented graphically on the matrix generated by the analyzer's software (Figure 5).

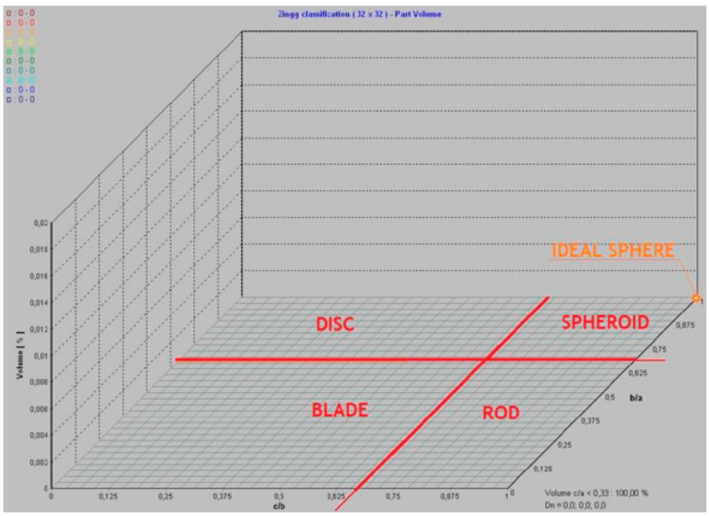

Figure 5. Zingg grain grouping matrix in the AWK 3D analyzer (source: www.kamika.pl/Analizator_P_AWK3D (accessed on 20 January 2022).

3. Discussion

3.1. Assessment of Grain Size Distribution

To assess the distribution of grain sizes measured by the dynamic 2D image analysis and by the 3D optoelectronic analysis, the shortest and longest grain dimensions recorded by both the measuring methods were used—these were the minimum Feret diameter (d_{Fmin}) for the 2D method and the width (b) for the 3D method. The longest grain dimensions were represented by the maximum Feret diameter (d_{Fmax}) for the 2D method and the length (a) for the 3D method. The results of the measurements in the form of the grain size curves for the two feeds and their enrichment products (I–IV) are shown in Figures 6 and 7. The grain size distributions of the feeds measured using sieves as the reference method are also given (Figure 6c). For description of particle size, the sieve diameter (d_{siev}) was used in this case. In order to compare the results obtained with the 2D and 3D methods, common particle dimensions corresponding to the given measurement method were marked on the X-axes $a/d_{Fmax}/b/d_{Fmin}/d_{siev}$.

The analysis of the grain size composition curves indicated that the consistency of the results for both the methods was different, depending on the defined grain dimension. The grain size distributions measured by the two methods were more consistent if the shortest grain dimensions are compared (Figure 6). At the same time, this was consistently higher for measurements of irregular grains. This is due to the fact that one of the three dimensions of an irregular grain is definitely shorter than that of a regular grain. In this case, the dynamic 2D image analysis method correctly identified the smallest dimensions of particles statistically more often due to their large population, approaching the results recorded by the 3D method (Figure 6b). Errors in identifying the shortest dimension of a free-moving particle by the 2D method were statistically greater for the population of regular grains, and in this case, the 2D method underestimated the share of fine grains (Figure 6a,c). The analysis of curves in the coarse grain range and the comparison with the research range of the grain class (6.3–8 mm) prepared using the sieves showed that both the methods, using the shortest grain criterion, registered grains as longer than 8 mm (Figure 6a,c). The grain sizes were overestimated because there were no grains with a shortest dimension of more than 8 mm in the test samples containing grains sized from

6.3 to 8 mm. It should be noted that the optoelectronic method overestimated the share of such larger grains to a much greater extent. Comparing the characteristics of the grain size distributions in the samples containing regular and irregular grains, using the shortest grain dimension (d_{Fmin}, b) criterion, it can be seen that the 3D optoelectronic method correctly registered regular grains over the entire grain size range as smaller in relation to regular grains (Figure 6c). This is also confirmed by the averaged smaller values of the characteristic grains, as summarized in Table 1. The dynamic 2D image analysis method correctly recorded the sizes of irregular grains as smaller than regular ones, but only within the range of fine grains. In the range of coarse grains (above dv 70%), it erroneously overestimated their sizes in relation to regular grains. This problem has been discussed in an earlier publication by the authors [53].

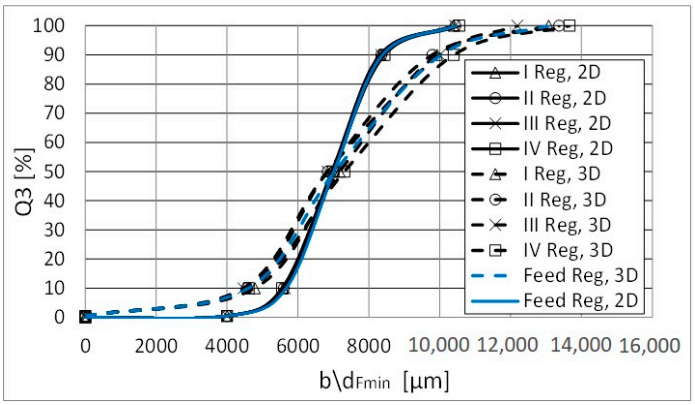

(**a**)

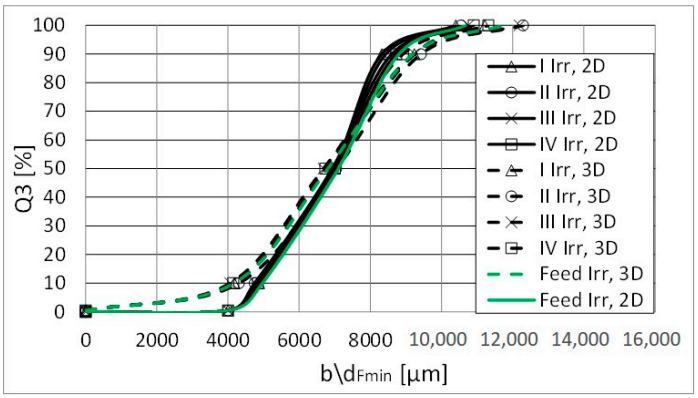

(**b**)

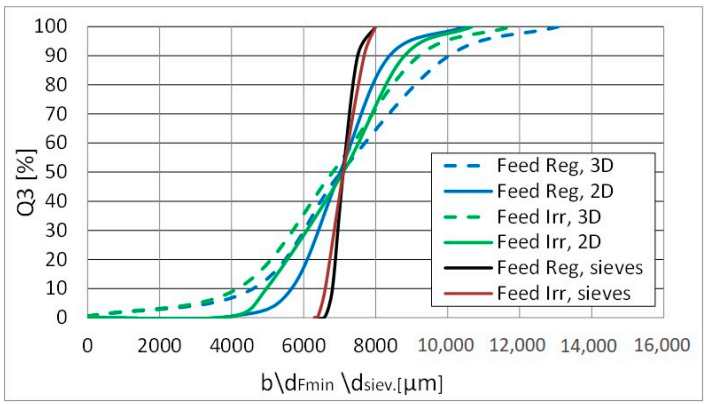

(**c**)

Figure 6. The grain size distributions in the test samples with regular and irregular grains, obtained by 2D and the 3D measuring methods, based on the shortest grain size criterion.

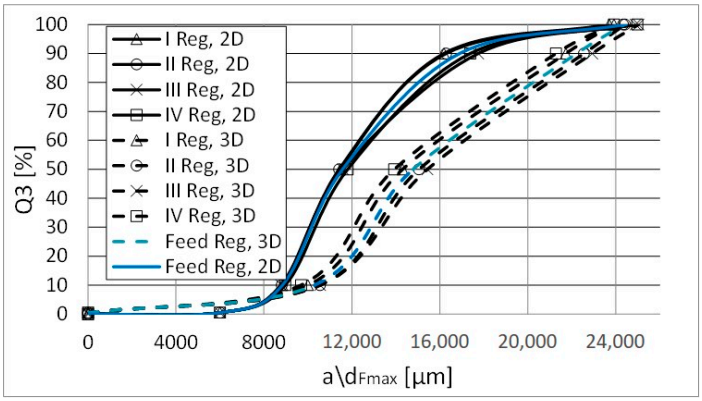

(**a**)

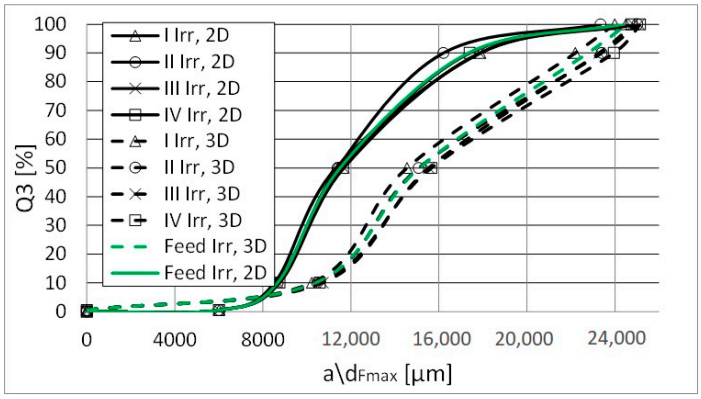

(**b**)

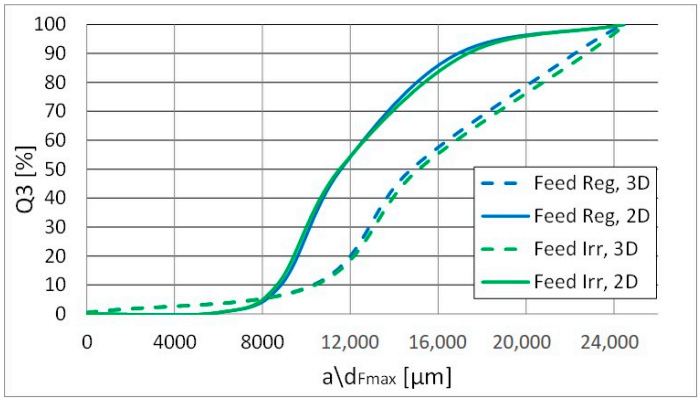

(**c**)

Figure 7. The grain size distributions in the test samples with regular and irregular grains, obtained by 2D and 3D measuring methods, based on the longest grain size criterion.

Table 1. The averaged characteristic grain sizes for the test samples and their standard deviations.

	3D		**2D**		**3D**		**2D**	
	***b*, Width**		***Fmin***		***a*, Length**		***Fmax***	
Q3 [%]	**Reg**	**Irr**	**Reg**	**Irr**	**Reg**	**Irr**	**Reg**	**Irr**
*dv*10 [µm]	4603 ± 134	4172 ± 103	5593 ± 34	4807 ± 61	10,195 ± 428	10,502 ± 208	8842 ± 87	8664 ± 99
*dv*50 [µm]	7038 ± 242	6805 ± 161	6984 ± 26	6963 ± 29	14,675 ± 686	15,206 ± 505	11,570 ± 174	11,509 ± 180
*dv*90 [µm]	10,028 ± 261	9203 ± 211	8364 ± 56	8521 ± 178	22,118 ± 753	23,210 ± 732	16,896 ± 763	17,335 ± 778

When the longest grain size (d_{Fmax}, a) is used to describe the grain size distribution, the discrepancy in the results between the measuring methods is very large (Figure 7). The underestimation of the share of grains measured by the longest dimension in the 2D method was statistically greater compared to the 3D method, which recorded the third dimension. This is due to the fact that grains filmed in random positions do not always show their longest dimension. Nevertheless, the size of the largest recorded grains was comparable in both methods and was about 24,500 µm. This behavior is consistent with the measurement statistics of a large population of particles. The above argumentation and the results achieved prove that the choice of a grain dimension estimator has a major impact on the characteristics of the measured grain size distribution. The use of the shortest grain dimension revealed differences in the grain size distributions of regular and irregular grains for both the measuring methods, while the use of the longest dimension as the estimator made it impossible to identify these differences within the same measuring method (Figures 6c and 7c).

Comparing the standard deviations of the measured characteristic grains $dv10$, $dv50$, $dv90$ in the tested samples for both the methods (Table 1) and the graphic course of the grain size curves (Figures 6 and 7), it can be clearly seen that the dynamic 2D image analysis method was more accurate; its standard deviations were characterized by lower values compared to those obtained by the optoelectronic method, both for regular and irregular grains.

The Span statistical index was used to determine the spread of the grain size distributions in the test samples. It was calculated based on the sizes of the characteristic grains d (percentiles of the grain size distribution $dv10$, $dv50$ and $dv90$). It give information on the width of the distribution and its skewness; the higher the value of the index, the wider the grain size distribution. With the same grain size ranges in the test samples, a lower Span value indicates greater deviations from the normal distribution (distribution skewness).

$$Span = \frac{dv90 - dv10}{dv50} \quad (3)$$

Table 2 summarizes the averaged Span indexes for the grain size distributions according to the shortest and longest dimensions of regular and irregular grains obtained by the 2D and the 3D methods. The higher index values showed wider grain size distributions obtained by the 3D optoelectronic method for both regular and irregular grains. Particularly large differences between the measuring methods were observed for distributions according to the shortest dimension (b, d_{Fmin}). As a rule, wider grain size distributions are obtained in measurements of irregular grains, except for grain size measurements using the 3D method according to the shortest dimension. In this case, the distributions of irregular grains were narrower than those of regular ones. This shows that the third grain dimension available in the 3D method made the identification of flat grains more accurate due to the precise recognition of their shapes.

Table 2. The averaged Span values for the particle grain size distributions obtained by the 2D and the 3D methods.

	3D		**2D**		**3D**		**2D**	
	***b*, Width**		F_{min}		***a*, Length**		F_{max}	
	Reg	**Irr**	**Reg**	**Irr**	**Reg**	**Irr**	**Reg**	**Irr**
Span	0.77	0.74	0.40	0.53	0.81	0.84	0.70	0.75

3.2. Evaluation of Grain Shapes

The shape factors dedicated to each of the measuring methods were used to compare differences in the shapes of regular and irregular grains. The circularity shape descriptor was used to assess the shapes of grains measured by the dynamic 2D image analysis

method and the sphericity was used to assess the shapes of grains measured with the 3D optoelectronic analyzer. Although both the factors belong to different classes of descriptors (*C*—class 2D, *S*—class 3D), they share common qualitative and quantitative information on the roundness of particles. In general, for particles of an elongated or flattened shape, the sphericity and circularity values decrease, and for ideally round particles, their values are equal to 1.

The comparison of the distribution curves of the shape factors of regular and irregular grains shown in Figure 8 and the numerical values of these factors in the selected percentiles of the distribution (Table 3) clearly show differences in the shapes of these grains. The values of the shape factors for irregular grains were significantly lower than the values of the factors for regular grains in both the measuring methods. It should be noted, however, that the 3D optoelectronic method—using the 3D class descriptor (sphericity)—better differentiated shapes of regular and irregular grains than the dynamic image analysis method using the 2D shape descriptor. The sphericity factor values for regular grains were smaller by about 12% than for regular grains, on average. This difference persisted over the entire range of the distribution of the factor (Figure 8b). The difference in the case of the circularity factor calculated for regular and irregular grains measured by the dynamic image analysis method was clearly smaller—about 3.5% on average. In addition, this difference was not constant over the whole distribution range of the circularity factor (Figure 8a). This means that the efficiency of differentiating grain shapes using the 2D method and the circularity factor depends on the grain flatness.

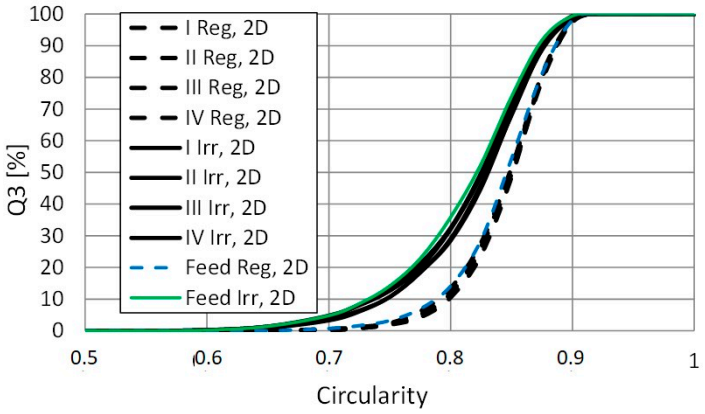

(**a**)

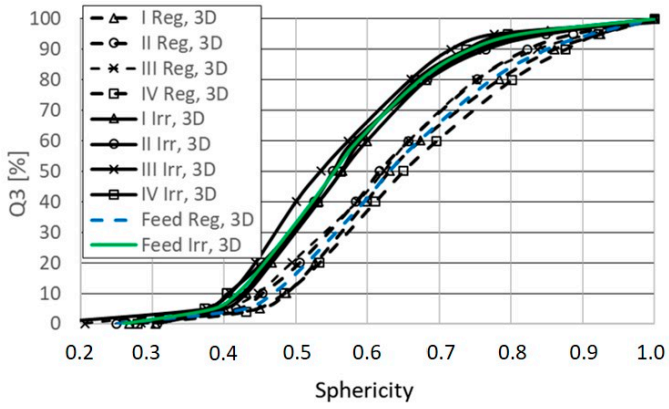

(**b**)

Figure 8. The distributions of shape factors in the test samples with regular and irregular grains, obtained by the 2D and the 3D measuring methods.

Table 3. The averaged particle shape factors obtained by the 2D and 3D methods and their standard deviations.

	3D		2D	
	Sphericity (*S*)		Circularity (*C*)	
Q3 [%]	Reg	Irr	Reg	Irr
10	0.47 ± 0.020	0.42 ± 0.013	0.80 ± 0.0037	0.75 ± 0.0064
50	0.63 ± 0.015	0.55 ± 0.014	0.85 ± 0.0013	0.83 ± 0.0030
90	0.85 ± 0.024	0.74 ± 0.012	0.89 ± 0.0011	0.87 ± 0.0016

By comparing the standard deviations of the calculated shape factors at the characteristic points of the distribution (10%, 50% and 90%) for both the measuring methods (Table 3), as well as the graphic course of their distributions (Figure 8), the greater measuring accuracy of the dynamic 2D image analysis method was confirmed. Its standard deviations were characterized by lower values compared to those obtained by the 3D optoelectronic method.

The nature of the relationships between the factors was examined in order to confirm the legitimacy of using different classes of shape factors to directly compare irregularities of grains measured by different measurement techniques (2D and 3D). The regression analysis comparing the shape factors showed a strong correlation (expressed by the coefficient of determination, R^2) and a linear relationship, which confirmed the possibility of their direct comparison and, on this basis, of finding differences in grain shapes (especially in flatness). The relationship between the shape factors took the form of the following equations: for regular grains: Circularity = 0.697 + 0.226 × Sphericity ± 0.010 (R^2 = 0.97); for irregular grains: Circularity = 0.596 + 0.386 × Sphericity ± 0.016 (R^2 = 0.96).

The sphericity factor used to compare the shapes of regular and irregular grains measured by the optoelectronic method, as shown by other authors [67], generally differentiated particles of different shapes well. However, it cannot distinguish shapes when the product of the shortest (*b*) and the intermediate (*c*) dimensions of the particle is similar. In this case, a flat disk can have the same value as an equiaxial rod. It is therefore good practice to use the sphericity (*S*) factor, as used in this research, in combination with a Zingg shape classification matrix (Figure 5). This is how the optoelectronic analyzer used in this research presented the shapes of particles, among other differences.

Figures 9 and 10 summarize the percentages of regular and irregular particles in the individual groups of shapes and Table 4 shows the averaged values. The analysis of the graphic and numerical results clearly reveals differences in the shapes of the measured regular and irregular grains. Irregular grains classified as spheres were definitely less numerous (6.5%) than regular grains assigned as spheres (20.4%) and, similarly, there were more blade-shaped grains (37.9%) among irregular than among regular grains (22.3%).

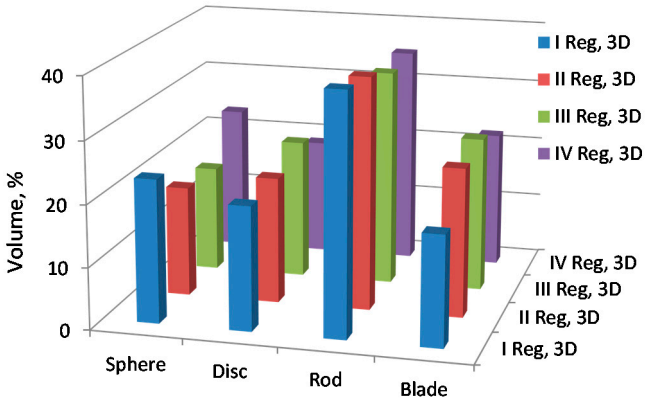

Figure 9. The distribution of grain shapes according to Zingg classification, obtained by the optoelectronic 3D method for the samples of regular grains.

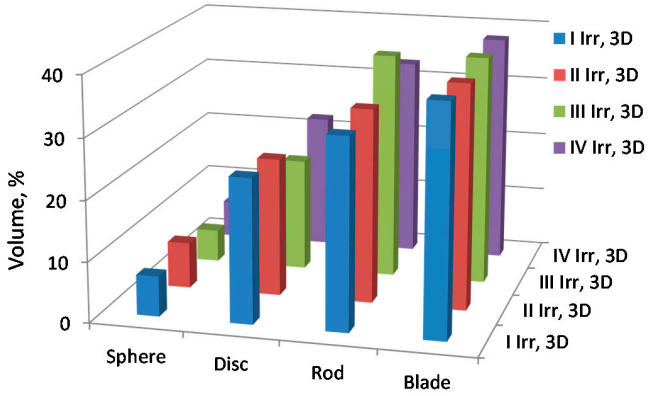

Figure 10. The distribution of grain shapes according to Zingg classification, obtained by the optoelectronic 3D method for the samples of irregular grains.

Table 4. The shares of grains of specific shapes determined by the 3D optoelectronic method.

Shape	Feed Reg %	Feed Irr %
Sphere	20.4	6.5
Disc	20.5	22.0
Rod	36.8	33.7
Blade	22.3	37.9

4. Conclusions

Based on the results of this research, the dynamic 2D image analysis method turned out to be more accurate compared to the 3D optoelectronic method. The 2D measurements of grain sizes, both regular and irregular, as well as the calculated shape factors, were burdened with smaller standard deviations than in the 3D method.

The choice of the grain size estimator had a major influence on the grain size distribution measurement outcome. The shortest grain size allowed for the effective differentiation of grain sizes between regular and irregular grains, in contrast to, for example, the longest grain dimension—the use of which makes it impossible to identify regular and irregular grains. The 3D method has turned out to be a more effective method for measuring the sizes of irregular particles; it more accurately sized large irregular grains based on their shortest dimension. Unlike the 2D method, it did not overestimate the sizes of large irregular particles. It seems, therefore, that measurements of the sizes and shapes of irregular (strongly flat) grains should be carried out, as far as possible, by the 3D technique. The use of the dynamic 2D image analysis technique for this purpose, as evidenced by the above studies, makes it possible to reliably find differences in the geometries of these grains and to obtain representative results—provided, however, that a large population of particles is ensured.

The regression analysis performed for the circularity and sphericity descriptors showed a strong linear correlation between them ($R^2 > 0.96$). Therefore, the correctness of the new approach—consisting of the use of different classes of shape descriptors adapted to the spatial class of the grain sizing by the specific measuring method—in unifying the results of measurements of grain shapes obtained by various measuring methods (2D and 3D) has been confirmed.

The methodology for the classification of grain shapes according to Zingg, used by an optoelectronic analyzer working in the infrared light range and dimensioning grains in an indirect way, enabled the effective identification of conventional grain shapes and their assignment to one of the four 3D spatial groups. The dynamic 2D image analysis method, unlike the 3D optoelectronic method, records physical images of particles. Therefore, it allows a more detailed analysis of the geometries of particles—in particular, the morphologies of their surfaces—using various estimators of the form and surface of the particles.

Author Contributions: Conceptualization: D.K. and T.G.; methodology, D.K.; formal analysis: A.K.; investigations: D.K., A.K. and T.G.; writing—original draft preparation: D.K.; writing—review and editing: A.K.; visualization: A.K.; supervision: D.K. All authors have read and agreed to the published version of the manuscript.

Funding: The article was written within the frame of a national Polish project granted by the Polish Research Centre: Artykuł jest wynikiem realizacji projektu w ramach konkursu NCBiR: konkursu nr 1 w ramach Poddziałania 4.1.4 "Projekty aplikacyjne" POIR w 2017 r., pt.: Opracowanie i budowa zestawu prototypowych urządzeń technologicznych do budowy innowacyjnego układu technologicznego do uszlachetniania kruszyw mineralnych wraz z przeprowadzeniem ich testów w warunkach zbliżonych do rzeczywistych". Projekt współfinansowany przez Unię Europejską ze środków Europejskiego Funduszu Rozwoju Regionalnego w ramach Działania 4.1 Programu Operacyjnego Inteligentny Rozwój 2014–2020.

Data Availability Statement: Not applicable.

Conflicts of Interest: The authors declare no conflict of interest.

References

1. *EN 933-3:2012*; Tests for Geometrical Properties of Aggregates-Part 3: Determination of Particle Shape-Flakiness Index. CEN European Committee for Standarization: Brussels, Belgium, 2012.
2. *EN 933-4:2008*; Tests for Geometrical Properties of Aggregates-Part 4: Determination of Particle Shape-Shape Index. European Committee for Standarization: Brussels, Belgium, 2008.
3. Zieliński, Z. *Korelacja Parametrów Technologicznych Mechanicznego Kruszenia i Przesiewania Materiałów Skalnych Stosowanych w Budownictwie Drogowym*; Wydawnictwo Uczelniane Politechniki Szczecińskiej: Szczecin, Poland, 1983; p. 228.
4. Tumidajski, T.; Naziemiec, Z. Wpływ warunków procesu kruszenia na kształt ziaren kruszyw mineralnych. In Proceedings of the IV Konferencja Kruszywa Mineralne Surowce-Rynek-Technologie-Jakość, Szklarska Poręba, Poland, 14–16 April 2004; Wydawnictwo Politechnika Wrocławska: Wrocław, Poland, 2004.
5. Naziemiec, Z.; Gawenda, T. Ocena efektów rozdrabniania surowców mineralnych w różnych urządzeniach kruszących. In Proceedings of the VI Konferencja, Kruszywa Mineralne–Surowce–Rynek–Technologie–Jakoś, Szklarska Poręba, Poland, 26–28 April 2006; OWPW: Wrocław, Poland, 2006; pp. 83–94.
6. Neville, A.M. *Właściwości Betonu*, 4th ed.; Polski Cement: Kraków, Poland, 2000.
7. Malewski, J. Kształt ziaren w produktach kruszenia. *Kruszywa* **2014**, *3*, 52–55.
8. Gawenda, T. Innowacyjne technologie produkcji kruszyw o ziarnach foremnych. Prace Naukowe Instytutu Górnictwa Politechniki Wrocławskiej. *Górnictwo Geol.* **2015**, *22*, 45–59.
9. Gawenda, T. *Zasady Doboru Kruszarek Oraz Układów Technologicznych w Produkcji Kruszyw Łamanych*; AGH University of Science and Technology Press: Cracow, Poland, 2015; pp. 1–232.
10. Mitchell, J.K.; Soga, K. *Fundamentals of Soil Behavior*, 3rd ed.; Wiley: New York, NY, USA, 2005; ISBN 978-0-471-46302-3.
11. Cho, G.-C.; Dodds, J.; Santamarina, J.C. Particle Shape Effects on Packing Density, Stiffness, and Strength: Natural and Crushed Sands. *J. Geotech. Geoenviron. Eng.* **2006**, *132*, 591–602. [CrossRef]
12. Pestana, J.M.; Whittle, A.J. Compression model for cohesionless soils. *Géotechnique* **1995**, *45*, 611–631. [CrossRef]
13. Rousé, P.C.; Fannin, R.J.; Shuttle, D.A. Influence of roundness on the void ratio and strength of uniform sand. *Géotechnique* **2008**, *58*, 227–231. [CrossRef]
14. Bessa, I.S.; Branco, V.T.F.C.; Soares, J.B.; Neto, J.A.N. Aggregate Shape Properties and Their Influence on the Behavior of Hot-Mix Asphalt. *J. Mater. Civ. Eng.* **2015**, *27*, 4014212. [CrossRef]
15. Connolly, B.J.; Loth, E.; Smith, C.F. Shape and drag of irregular angular particles and test dust. *Powder Technol.* **2020**, *363*, 275–285. [CrossRef]
16. KKnoll, M.; Gerhardter, H.; Prieler, R.; Mühlböck, M.; Tomazic, P.; Hochenauer, C. Particle classification and drag coefficients of irregularly-shaped combustion residues with various size and shape. *Powder Technol.* **2019**, *345*, 405–414. [CrossRef]
17. Krumbein, W.C. Settling-velocity and flume-behavior of non-spherical particles. *Trans. Am. Geophys. Union* **1942**, *23*, 621–633. [CrossRef]
18. Jonasz, M. Nonsphericity of suspended marine particles and its influence on light scattering1. *Limnol. Oceanogr.* **1987**, *32*, 1059–1065. [CrossRef]
19. Krawczykowski, D. Application of a vision systems for assessment of particle size and shape for mineral crushing products. *IOP Conf. Ser. Mater. Sci. Eng.* **2018**, *427*, 012013. [CrossRef]
20. Beuselinck, L.; Govers, G.; Poesen, J.; Degraer, G.; Froyen, L. Grain-size analysis by laser diffractometry: Comparison with the sieve-pipette method. *Catena* **1998**, *32*, 193–208. [CrossRef]
21. Li, M.; Wilkinson, D.; Patchigolla, K. Comparison of Particle Size Distributions Measured Using Different Techniques. *Part. Sci. Technol.* **2005**, *23*, 265–284. [CrossRef]

22. Xu, R.; Di Guida, O.A. Comparison of sizing small particles using different technologies. *Powder Technol.* **2003**, *132*, 145–153. [CrossRef]
23. Shang, Y.; Kaakinen, A.; Beets, C.J.; Prins, M.A. Aeolian silt transport processes as fingerprinted by dynamic image analysis of the grain size and shape characteristics of Chinese loess and Red Clay deposits. *Sediment. Geol.* **2018**, *375*, 36–48. [CrossRef]
24. Sneed, E.D.; Folk, R.L. Pebbles in the Lower Colorado River, Texas a Study in Particle Morphogenesis. *J. Geol.* **1958**, *66*, 114–150. [CrossRef]
25. Krumbein, W.C. Measurement and Geological Significance of Shape and Roundness of Sedimentary Particles. *J. Sediment. Res.* **1941**, *11*, 64–72. [CrossRef]
26. Wentworth, C.K. *The Shapes of Beach Pebbles. US Geological Survey Professional Paper*; US Government Printing Office: Washington, DC, USA, 1922; Volume 131, pp. 75–83.
27. Zingg, T. Beitrag zur Schotteranalyse. Schweizer Miner. *Petrog. Mitt.* **1935**, *15*, 39–140.
28. Allen, T. *Powder Sampling and Particle Size Determination*, 1st ed.; Elsevier Science: London, UK, 2003; ISBN 9780080539324.
29. Rodriguez, J.; Edeskär, T.; Knutsson, S. Particle shape quantities and measurement techniques: A review. *Electron. J. Geotech. Eng.* **2013**, *18*, 169–198.
30. Krawczykowski, D. *Unification of the Results of Granulometric Analyzes of Finegrained Mineral Powders*; Dissertations and Monographs 347; AGH University of Science and Technology: Krakow, Poland, 2019.
31. Illenberger, W.K. Pebble Shape (and Size!). *J. Sediment. Res.* **1991**, *61*, 756–767.
32. Bott, S.J.; Pye, K. Particle shape: A review and new methods of characterization and classification. *Sedimentology* **2008**, *55*, 31–63.
33. Freund, Y.; Schapire, R.E. A Decision-Theoretic Generalization of On-Line Learning and an Application to Boosting. *J. Comput. Syst. Sci.* **1997**, *55*, 119–139. [CrossRef]
34. Zheng, J.; Hryciw, R.D. Identification and Characterization of Particle Shapes from Images of Sand Assemblies Using Pattern Recognition. *J. Comput. Civ. Eng.* **2018**, *32*, 04018016. [CrossRef]
35. Liang, Z.; Nie, Z.; An, A.; Gong, J.; Wang, X. A particle shape extraction and evaluation method using a deep convolutional neural network and digital image processing. *Powder Technol.* **2019**, *353*, 156–170. [CrossRef]
36. Riley, C.M.; Rose, W.I.; Bluth, G.J.S. Quantitative shape measurements of distal volcanic ash. *J. Geophys. Res. Earth Surf.* **2003**, *108*, 2504. [CrossRef]
37. Taylor, M.; Garboczi, E.; Erdogan, S.; Fowler, D. Some properties of irregular 3-D particles. *Powder Technol.* **2006**, *162*, 1–15. [CrossRef]
38. Alfano, F.; Bonadonna, C.; Delmelle, P.; Costantini, L. Insights on tephra settling velocity from morphological observations. *J. Volcanol. Geotherm. Res.* **2011**, *208*, 86–98. [CrossRef]
39. Lin, C.; Miller, J. 3D characterization and analysis of particle shape using X-ray microtomography (XMT). *Powder Technol.* **2005**, *154*, 61–69. [CrossRef]
40. Ersoy, O.; Şen, E.; Aydar, E.; Tatar, İ.; Çelik, H.H. Surface area and volumemeasurements of volcanic ash particles using micro-computed tomography (micro-CT): A comparison with scanning electron microscope (SEM) stereoscopic imaging and geometric considerations. *J. Volcanol. Geotherm. Res.* **2010**, *196*, 281–286. [CrossRef]
41. Mills, O.P.; Rose, W.I. Shape and surface area measurements using scanning elektron microscope stereo-pair images of volcanic ash particles. *Geosphere* **2010**, *6*, 805–811. [CrossRef]
42. Asahina, D.; Taylor, M. Geometry of irregular particles: Direct surface measurements by 3-D laser scanner. *Powder Technol.* **2011**, *213*, 70–78. [CrossRef]
43. Garboczi, E.; Liu, X.; Taylor, M. The 3-D shape of blasted and crushed rocks: From 20µm to 38mm. *Powder Technol.* **2012**, *229*, 84–89. [CrossRef]
44. Ersoy, O. Surface area and volume measurements of volcanic ash particles by SEM stereoscopic imaging. *J. Volcanol. Geotherm. Res.* **2010**, *190*, 290–296. [CrossRef]
45. Bullard, J.W.; Garboczi, E.J. Defining shape measures for 3D star-shaped particles: Sphericity, roundness, and dimensions. *Powder Technol.* **2013**, *249*, 241–252. [CrossRef]
46. White, D.J. PSD measurement using the single particle optical sizing (SPOS) method. *Geotechnique* **2003**, *53*, 317–326. [CrossRef]
47. Altuhafi, F.; O'Sullivan, C.; Cavarretta, I. Analysis of an Image-Based Method to Quantify the Size and Shape of Sand Particles. *J. Geotech. Geoenviron. Eng.* **2013**, *139*, 1290–1307. [CrossRef]
48. Bowman, E.; Soga, K.; Drummond, W. Particle shape characterization using Fourier descriptor analysis. *Geotechnique* **2001**, *51*, 545–554. [CrossRef]
49. Sukumaran, B.; Ashmawy, A. Quantitative characterization of discrete particles. *Geotechnique* **2001**, *51*, 619–627. [CrossRef]
50. Garboczi, E.; Hrabe, N. Particle shape and size analysis for metal powders used for additive manufacturing: Technique description and application to two gas-atomized and plasma-atomized Ti64 powders. *Addit. Manuf.* **2020**, *31*, 100965. [CrossRef]
51. Bay, B.K.; Smith, T.S.; Fyhrie, D.P.; Saad, M. Digital volume correlation: Three-dimensional strain mapping using X-ray tomography. *Exp. Mech.* **1999**, *39*, 217–226. [CrossRef]
52. Gawenda, T.; Saramak, D.; Nad, A.; Surowiak, A.; Krawczykowska, A.; Foszcz, D. Badania procesu uszlachetniania kruszyw w innowacyjnym układzie technologicznym. In Proceedings of the XIX Konferencja Kruszywa Mineralne Surowce-Rynek-Technologie-Jakość, Kudowa Zdrój, Poland, 24–26 April 2019.

53. Gawenda, T.; Krawczykowski, D.; Krawczykowska, A.; Saramak, A.; Nad, A. Application of Dynamic Analysis Methods into Assessment of Geometric Properties of Chalcedonite Aggregates Obtained by Means of Gravitational Upgrading Operations. *Minerals* **2020**, *10*, 180. [CrossRef]
54. Bagheri, G.H.; Bonadonna, C.; Manzella, I.; Vonlanthen, P. On the characterization of size and shape of irregular particles. *Powder Technol.* **2015**, *270*, 141–153. [CrossRef]
55. Krumbein, W.C.; Sloss, L.L. *Stratigraphy and Sedimentation*; W.H. Freeman and Company: San Francisco, CA, USA, 1951.
56. Mora, C.F.; Kwan, A.K.H. Sphericity, shape factor, and convexity measurement of coarse aggregate for concrete using digital image processing. *Cem. Concr. Res.* **2000**, *30*, 351–358. [CrossRef]
57. Riley, N.A. Projection sphericity. *J. Sediment. Res.* **1941**, *11*, 94–95. [CrossRef]
58. Wadell, H. Sphericity and Roundness of Rock Particles. *J. Geol.* **1933**, *41*, 310–331. [CrossRef]
59. Santamarina, J.C.; Cho, G.C. Soil behaviour: The role of particle shape. In *Advances in Geotechnical Engineering: The Skempton Conference*; Thomas Telford Publishing: London, UK, 2004; pp. 604–617.
60. Kuo, C.-Y.; Freeman, R.B. Imaging Indices for Quantification of Shape, Angularity, and Surface Texture of Aggregates. *Transp. Res. Rec. J. Transp. Res. Board* **2000**, *1721*, 57–65. [CrossRef]
61. Wadell, H. Volume, Shape, and Roundness of Rock Particles. *J. Geol.* **1932**, *40*, 443–451. [CrossRef]
62. Mandelbrot, B. How Long Is the Coast of Britain? Statistical Self-Similarity and Fractional Dimension. *Science* **1967**, *156*, 636–638. [CrossRef]
63. Cox, E.P. A method of assigning numerical and percentage values to the degree of roundness of sand grains. *J. Paleontol.* **1927**, *1*, 179–183.
64. Su, D.; Yan, W.M. 3D characterization of general-shape sand particles using microfocus X-ray computed tomography and spherical harmonic functions, and particle regeneration using multivariate random vector. *Powder Technol.* **2018**, *323*, 8–23. [CrossRef]
65. Yan, P.; Zhang, J.; Fang, Q.; Zhang, Y.; Fan, J. 3D numerical modelling of solid particles with randomness in shape considering convexity and concavity. *Powder Technol.* **2016**, *301*, 131–140. [CrossRef]
66. Zhao, B.; Wang, J. 3D quantitative shape analysis on form, roundness, and compactness with μCT. *Powder Technol.* **2016**, *291*, 262–275. [CrossRef]
67. Al-Rousan, T.; Masad, E.; Tutumluer, E.; Pan, T. Evaluation of image analysis techniquesfor quantifying aggregate shape characteristics. *Constr. Build. Mater.* **2007**, *21*, 978–990. [CrossRef]